Journal Name

ARTICLE TYPE

Cite this: DOI: 00.0000/xxxxxxxxxx

Supplementary information for reduction of NO_x on metal-free hydrogenated hexagonal boron nitride.†

Anthony J. R. Payne[a], Neubi F. Xavier Jr[a] and, Marco Sacchi[a].

Received Date
Accepted Date

DOI: 00.0000/xxxxxxxxxx

To compare the results of our approach to the literature, we consider the work of Surya et al..[1] **Table S1** compares the formation energies of V_N and 1-3HV_N and shows excellent agreement with the exception of 2HV_N. Here, we explored geometries where hydrogen is positioned on the same side of the hBN plane and on alternate sides of the plane and found an E_f of 7.29 eV and 6.86 eV for hydrogen atoms on the same side and opposite sides of the plane, respectively. This discrepancy in energy can be explained by the greater steric hindrance of hydrogens on the same side of the plane, reducing the stability of the 2HV_N vacancy. **Figure S1** shows two of the geometries of the 2HV_N vacancy.

System	This study	Surya et. al.[1]
V_N	8.63	8.69
1HV_N	6.93	6.94
2HV_N(H Same side)	7.29	7.38
2HV_N(H opposite side)	6.86	-
3HV_N	5.29	5.27

Table S1: Formation energies (eV) of V_N and 1-3HV_N vacancies.

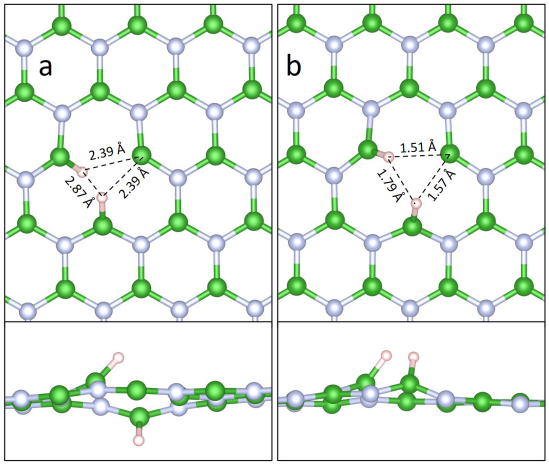

Fig. S1 Geometries of the 2HV_N vacancy, (a) 2$HV_N$with Hydrogen atoms on opposite sides of the hBN plane with an E_f of 6.86 eV and (b) 2$HV_N$with Hydrogen atoms on the same side of the hBN plane with an E_f of 7.29 eV.

E-mail:m.sacchi@surrey.ac.uk, apayne@surrey.ac.uk
[a] *Department of Chemistry, University of Surrey, Guildford, GU2 7XH, UK.*

The Gibbs free energy (G) was determined utilising the fundamental equation G = H - TS, where S represents entropy, and H is the enthalpy. H includes the DFT energy at 0 K, the zero-point energy correction, and the thermal contributions from translational, rotational, and vibrational energy changes to the internal energy (U). S consists of rotational, translational, and vibrational entropy, calculated using partition functions. For gas-phase species, the translational and rotational contributions are added according to the ideal gas statistical thermodynamic laws, whereas for the solid-phase species, only the vibrational contributions are considered. G was then used to calculate the Gibbs free energy of formation (G_f) for using the equation:

$$G_f = G_V - G_{hBN} + \frac{1}{2}n_N G_{N_2} + n_B G_B - \frac{1}{2}n_H G_{H_2} \tag{1}$$

The G_f for the defect structures discussed in the main text are presented in **Figure S2**. Notably, the G_f increases with temperature for defects containing a higher number of hydrogen atoms. Among the vacancies investigated, $3HV_B$ is the most stable defect across the temperature range from 25 K to 1000 K, followed by $2HV_B$. Both $3HV_N$ and N_B show a similar trend, with G_f increasing with temperature. In contrast, the G_f of $1HV_N$ slightly decreases with temperature, reaching a value of 6.64 eV at 1000 K, comparable to that of $3HV_N$ and N_B. At lower temperatures, $1HV_B$ and $2HV_N$ have similar G_f values, but as temperature increases, the G_f of $2HV_N$ rises, whilst for $1HV_B$ G_f falls. The G_f of V_N decreases with temperature, becoming lower than that of $2HV_N$ at temperatures above 938 K. V_B has the highest G_f throughout the temperature range, making it the least stable defect. Generally, defects with fewer hydrogen atoms experience a decrease in G_f with temperature, whereas defects with more hydrogen atoms increase. This trend is attributed to the significant increase in entropy for $\frac{1}{2}H_2$ compared to the hydrated defect. Overall, the stability order of defects aligns with their formation energy E_f, with $3HV_B$ emerging as the most stable defect from 25 K to 1000 K.

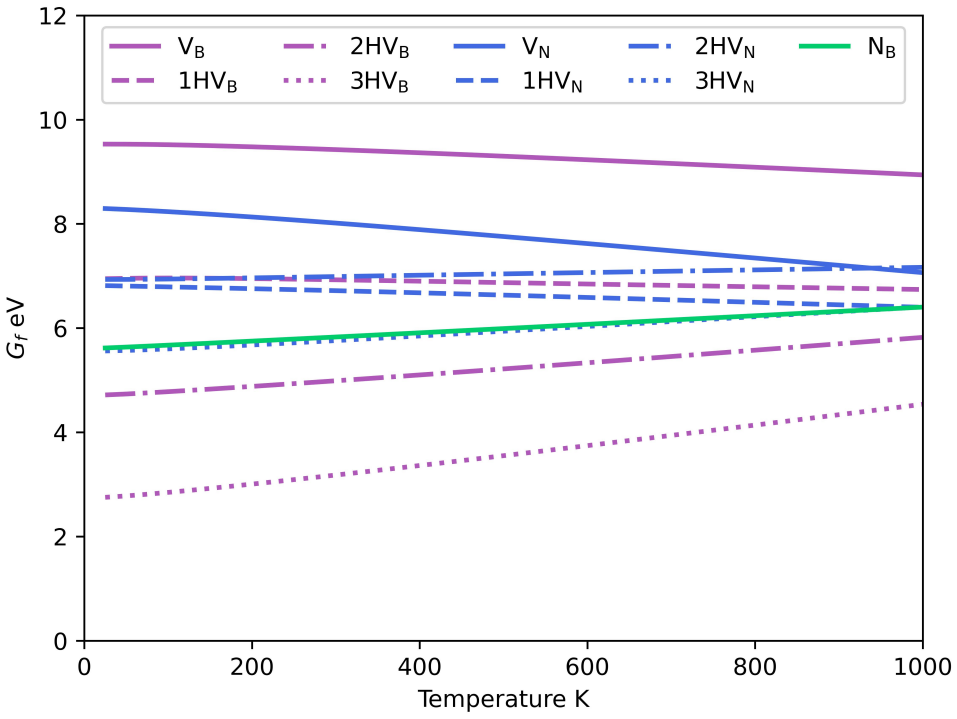

Fig. S2 Variation in Gibbs free energy of formation (G_f) with temperature for hBN defect structures.

In addition to temperature, partial pressures of gas-forming species influence G_f. The effect is captured by rewriting Equation 1 as follows:

$$G_f = G_V - G_{hBN} + \frac{1}{2}n_{N_2}\left(G_{N_2} + k_B T \ln\left(\frac{p_{N_2}}{p_0}\right)\right) + n_B G_B - \frac{1}{2}n_{H_2}\left(G_{H_2} + k_B T \ln\left(\frac{p_{H_2}}{p_0}\right)\right) \tag{2}$$

Where p_{N_2}, p_{H_2} is the partial pressure of N_2 and H_2, respectively. p_0 is a reference pressure. G values were selected for temperatures of 298 K and 1000 K with p_0 of 1 bar and 10 bar such that $p_0 = p_{N_2} + p_{H_2}$; results are shown in Figure S3.the G_f of hydrogen-containing defects show a slight downward trend with increasing p_{H_2} at at low p_{H_2} ranges. Furthermore, vacant nitrogen defects show a slight downward curvature with increasing p_{H_2} at high p_{H_2} ranges. In the middle of the range of p_{H_2}, the G_f remains quite constant. The

overall effect leads to a slight decrease in G_f with increasing p_{H_2} and, therefore, higher stability. The G_f exhibits greater variation at 1000 K than 298 K, with $3HV_N$ having a greater G_f than N_B at low p_{H_2}, with the 10 bar case compounding the effect. Despite the effect of pressure, the order of defect stability is largely unchanged, with $3HV_B$ remaining the most stable defect structure with the lowest G_f.

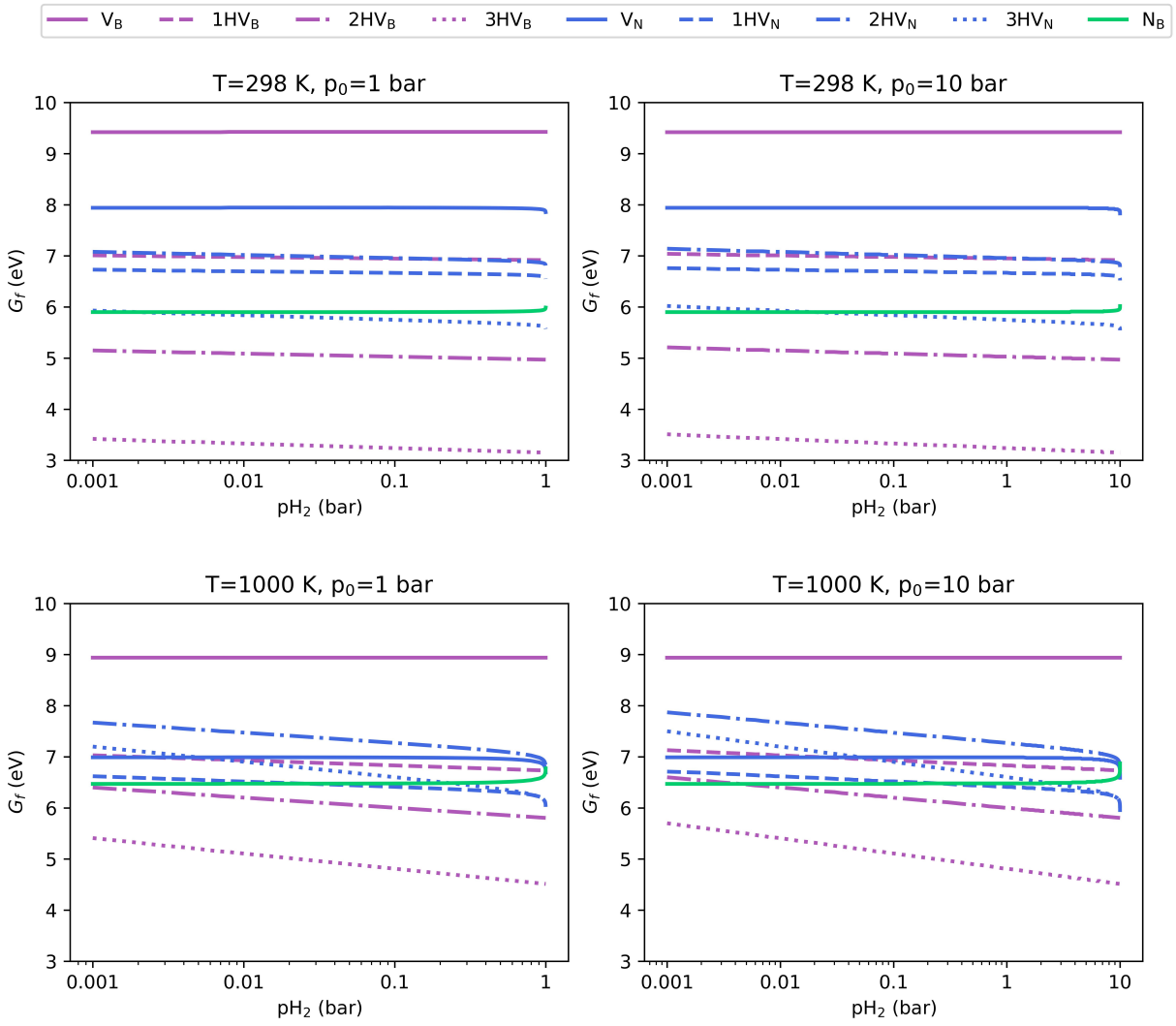

Fig. S3 Variation in Gibbs free energy of formation (G_f) with H_2 partial pressure (p_{H_2}) for hBN defect structures at 298 K and 1000 K.

0.1 Adsorption sites and reaction steps

The global minimum adsorption site for NO_2 was determined using the following approach. Single point energies were calculated for NO_2 in orientations and sites as shown in **Figure S4** for a range of heights from 2 Å to 4.5 Å above the hBN surface. The minimum energy structure at each position was then geometry optimised to find the adsorption energy with the minimum energy configuration shown in **2** of the main text. A similar procedure was used to identify the adsorption positions and orientation of NO_2 and NO above $3HV_B$ as illustrated in **Figure S4**.

The optimal adsorption site for NO_2 was determined through the following methodology. Initial single-point energy calculations were conducted for NO_2 across the orientations and sites depicted in **Figure S4**, with the molecule positioned at heights ranging from 2 Å to 4.5 Å above the hBN surface. The structures with the lowest energy at each position underwent geometry optimisation to ascertain the adsorption energy, ultimately leading to the determination of the minimum energy configuration, as illustrated in Figure 2 of the main text. A similar approach was employed to identify the adsorption positions and orientations of NO_2 and NO atop $3HV_B$, with sites and orientations shown in **Figure S4**.

Alternate reaction pathways for the reaction of NO_2 on $3HV_B$ were explored. Initiation of the hydrogen transfer step from $3HV_B$ to NO_2 to create a NO_2H intermediate (TS2, $3HV_B \rightleftharpoons NO_2H$) with NO_2 originating from different adsorption sites and orientations.

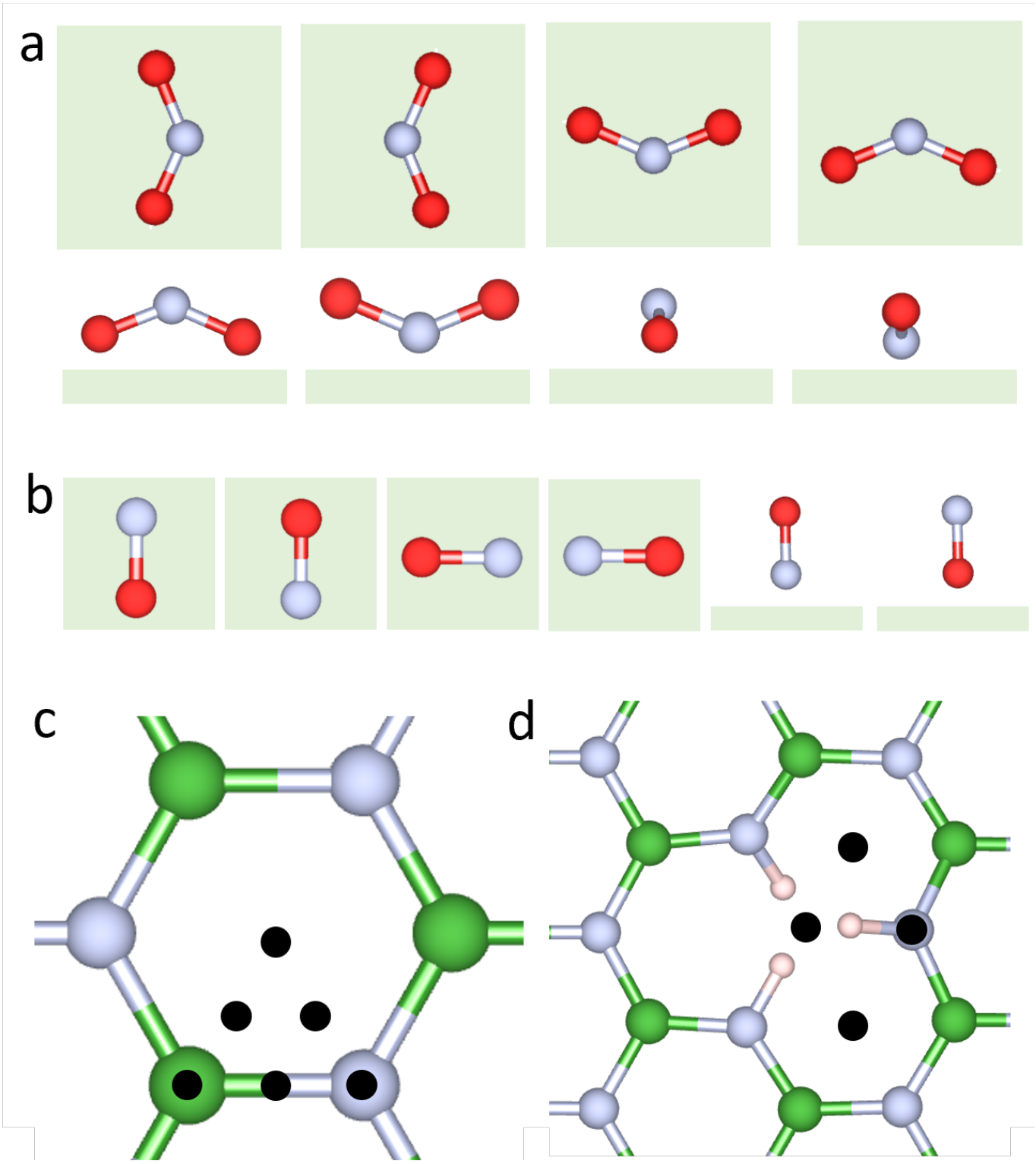

Fig. S4 (a) and (b) illustrate the orientations of NO2 and NO above the hBN/3HV$_B$ surface sites shown in (c)/(d). These orientations and sites are initially considered in the single-point energy calculations.

However, these attempts yielded higher energy barriers (>1.20 eV) compared to those presented in the main text. Combining TS3 and TS4 into a single step resulted in a slightly elevated energy barrier of 0.77 eV with geometry optimisation of the transition state, revealing a structure neither resembling the reactant nor the product, indicating the existence of a metastable rotation intermediate. As an alternative to TS5 (barrier of 0.96 eV), we explored breaking the N-OH bond to yield a hydroxyl group bound to the surface boron adjacent to the remaining NO ($NO_2H \rightleftharpoons NO + OH$). Subsequent steps involved moving the hydroxyl group closer to a surface H,

followed by the formation of H_2O. Despite the low barrier to breaking the N-OH bond (0.25 eV), the subsequent steps presented barriers of 1.16 eV and 1.27 eV. Further iterations to form the N_B site and produce the first water molecule also resulted in multistep reactions with large barriers. Consequently, TS5, with a single barrier of 0.96 eV, is the minimum energy pathway. Following the production of a water molecule, the resulting geometry offered fewer possible alternative routes and pathways to form the N_B site. Unlike NO_2 reaction, hydrogen transfer from $3V_B$ to NO form a physisorbed HNO species results in a metastable geometry with an energy of 2.20 eV; therefore, the chemisorption of NO occurs in a single step (TS11).

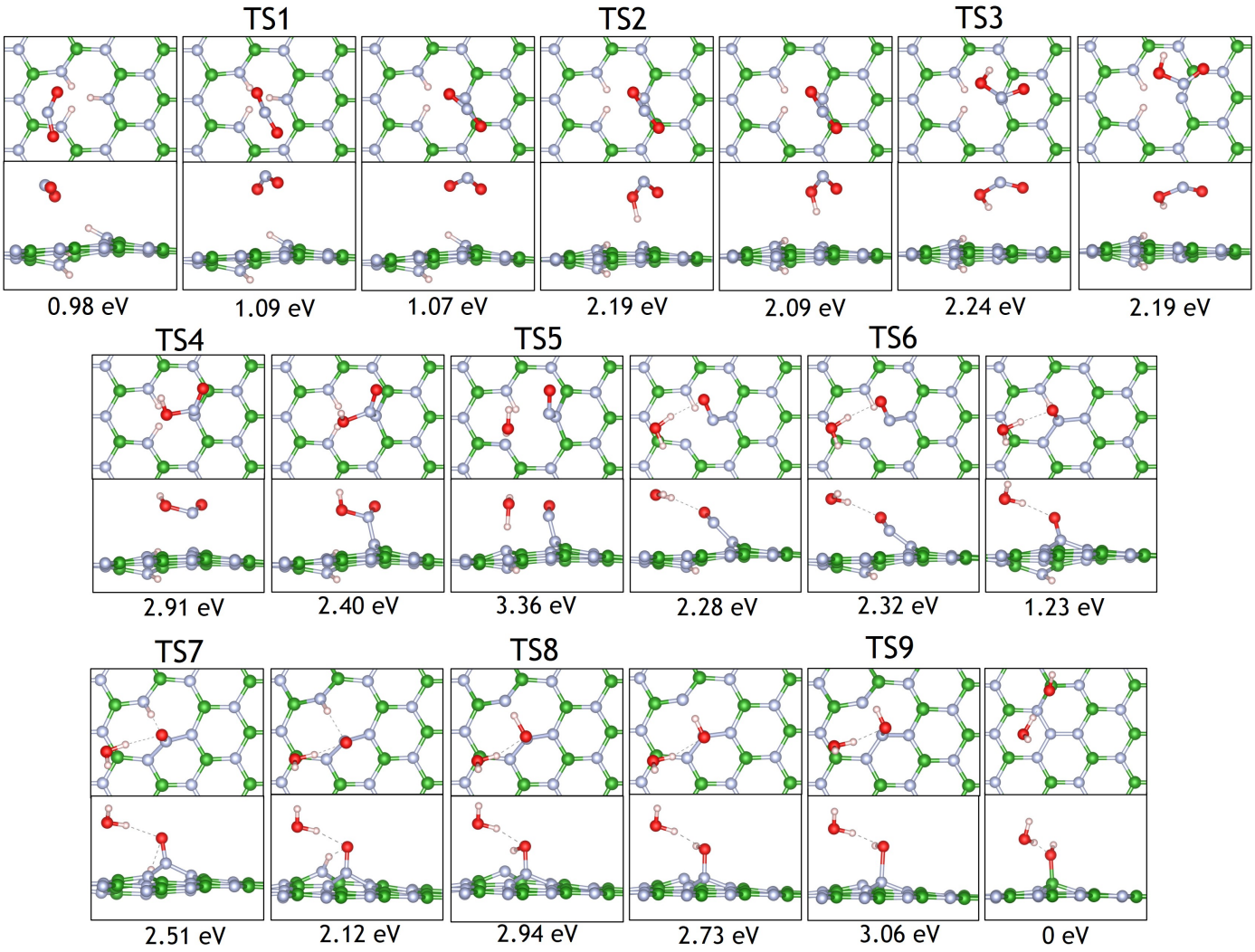

Fig. S5 Structures along the reaction coordinate for the reaction of NO_2 with $3HV_B$. Transition states are labelled TS1-9. The product of the reaction, a nitrogen antisite adjacent to a boron site with a hydroxyl group, is used as the reference energy.

0.2 Details of the microkinetic modelling

Kinetics simulations for the mechanism of NO_2 conversion into products were performed using MKMCXX.[2] The non-activated adsorption rate constant for the adsorbed NO_2 was calculated using Hertz-Knudsen kinetics (Equation 3 in the main text) with the surface area determined by the hydrogen atoms of the $3HV_B$ vacancy. The rate constants of the surface reaction steps with discrete transition states were calculated according to transition state theory in (Equation 4 in the main text), with Arrhenius parameters shown in **Table S2**. The combination of Hertz-Knudsen kinetics and transition state theory in microkinetic models has been successfully adopted in previous works.[3–6] As the barriers of TS1 and TS3 are negligible at higher temperatures, we decided to combine the TS1, TS2 and TS3 in a single step. A simulation time of 10000 s was set to allow for steady-state convergence, and the maximum absolute and relative tolerances were set to 1×10^{-16}. Reaction rates were then calculated as a function of temperature and are shown in the main text.

Figure S6 shows the effect of pressure on the consumption rate of NO_2 and H_2O production. Here, we can see the peak conversion rate occurs at decreasing temperatures as the pressure increases. As the pressure increases, higher coverages of NO_2 are achieved

Label	Arrhenius coefficient (s^{-1}) Forward	Reverse	Activation energy (eV) Forward	Reverse
TS1 - TS3	2.26E+13	6.11E+12	1.22	0.05
TS4	1.32E+12	2.26E+13	0.70	0.47
TS5	1.19E+14	3.17E+12	0.75	0.92
TS6	1.79E+13	1.01E+14	0.04	1.08
TS7	2.19E+13	6.84E+13	1.31	0.42
TS8	2.97E+13	2.84E+12	0.71	0.09
TS9	2.18E+13	1.60E+13	0.28	3.04
TS10	4.03E+12	3.02E+11	0.25	1.52

Table S2: Parameters for the elementary reactions involved in the microkinetic modelling of the reaction of NO_2 with $3HV_B$.

at lower temperatures per the adsorption isotherms,[7] therefore, the peak rate of NO_2 and H_2O production occurs at lower temperatures with increased pressure. The model has no competing reactions; therefore, the number of surface sites limits the rate of NO_2 consumption to 3.68×10^{-5} s^{-1} when assuming a 1:1 ratio of NO_2 to $3HV_B$ sites.

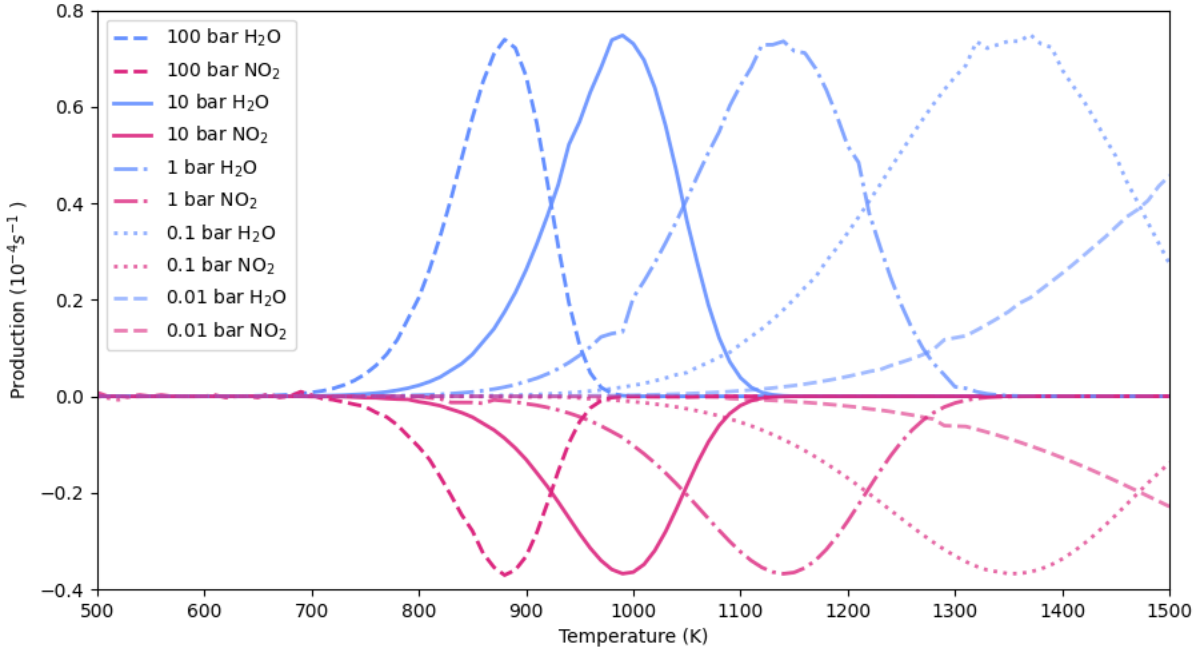

Fig. S6 The effect of pressure on the rate of NO_2 consumption and H_2O production at different temperatures. The rates reach their maximum at 880 K, 990 K, 1140 K and 1370 K for pressures of 100, 10, 1, 0.1 and 0.01 bar, respectively.

0.3 Formation of hydrogenated V_B defects

In order to confirm the likelihood of the formation of hydrogenated V_B defects when exposed to hydrogen, the reaction of H_2 with $1HV_B$ and $2HV_B$ was investigated. **Figure S7a** shows the reaction of $1HV_B$ with H_2. Physisorbed H_2 is dissociated into two separate H atoms, overcoming an energy barrier of 1.47 eV, forming N-B bonds. The surface hydrogen atoms undergo a subsequent rearrangement step to find the minimum energy $3HV_B$ configuration. The overall reaction has a ΔE of -4.77 eV. Given the high barrier for the reverse reaction (5.98 eV), the reverse reaction is unlikely even at high temperatures. The reaction of $2HV_B$ with H_2 is shown in **Figure S7b**, here H_2 is dissociated to form a $3HV_B$ with a hydrogen atom adsorbed onto an adjacent boron site. This reaction has a barrier of 0.92 eV and may provide a source of hydrogen atoms on the surface for reactions such as TS10 of the main text.

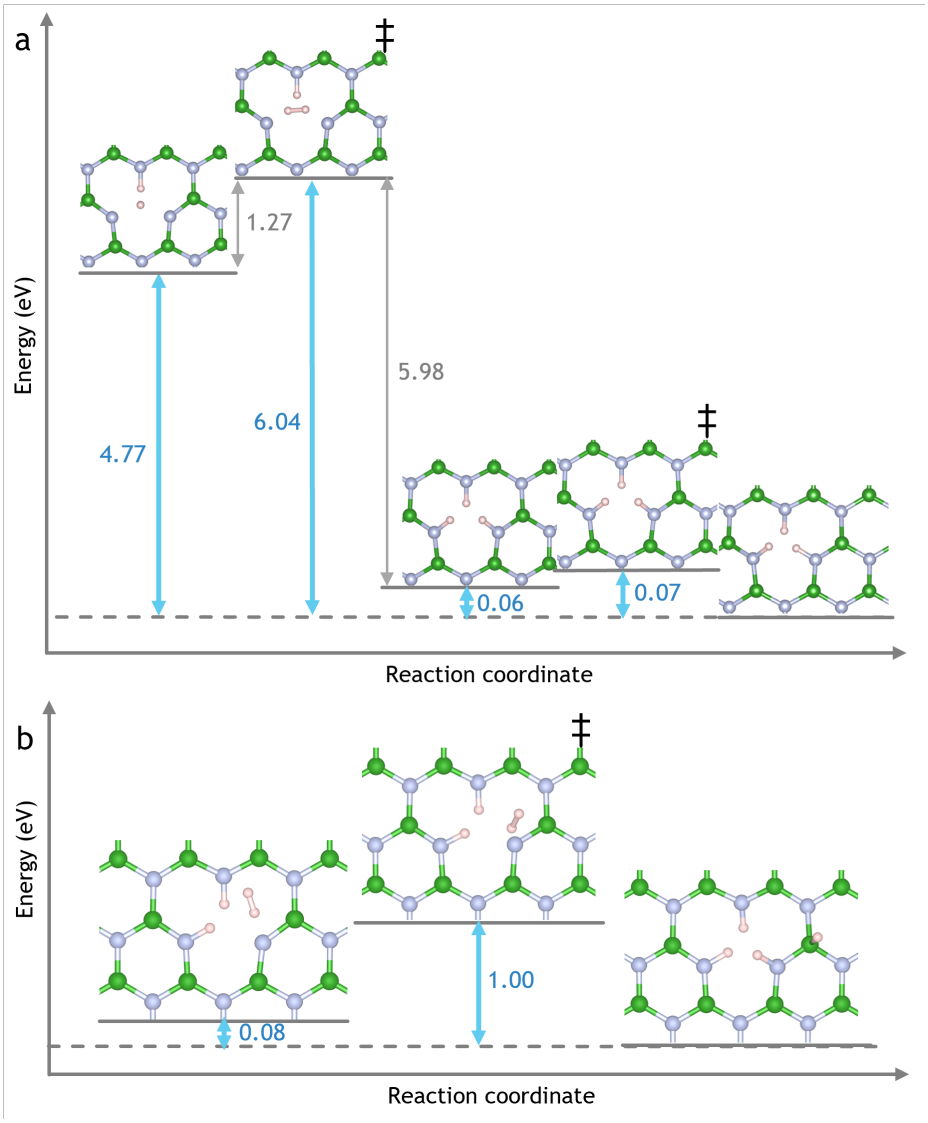

Fig. S7 (a) The reaction of $1HV_B$ with H_2, the product of the reaction is a $3HV_B$, the reaction has a ΔE of -4.77 eV with a transition state barrier of 1.47 eV. (b) The reaction of $2HV_B$ with H_2, the product of the reaction is a $3HV_B$ with a hydrogen atom adsorbed onto an adjacent boron site.

Notes and references

1 V. Surya, K. Choutipalli, K. Esackraj and E. Varathan, *Applied Surface Science*, 2022, **602**, 15.

2 I. A. Filot, R. A. Van Santen and E. J. Hensen, *Angewandte Chemie - International Edition*, 2014, **53**, 12746–12750.

3 N. F. Xavier, G. F. Bauerfeldt and M. Sacchi, *ACS Applied Materials and Interfaces*, 2023, **15**, 6951–6962.

4 H. Ma and W. F. Schneider, *ACS Catalysis*, 2019, **9**, 2407–2414.

5 Z. Lian, C. Si, F. Jan, M. Yang and B. Li, *ACS Catalysis*, 2020, **10**, 14006–14014.

6 L. Foppa, M.-C. Silaghi, K. Larmier and A. Comas-Vives, *Journal of Catalysis*, 2016, **343**, 196–207.

7 G. Attard and C. Barnes, *Surfaces (Oxford Chemistry Primer)*, 1998.